International Journal of Nanomedicine

Dovepress
Taylor & Francis Group

Open Access Full Text Article

ORIGINAL RESEARCH

Folate-Modified Smart Responsive Nanosystems for Enhancing Anti-Tumor Therapy Through Calcium Overload and Chemotherapy

Yongcheng Tang[1,2,*], Jingrong Huang[3,*], Cheng Cui[1,2], Fengyi Yang[1,2], Kaifu Li[1,2], Benjian Gao[1,2], Shaozhi Fu[3], Xiaoli Yang[1,2]

[1]Department of General Surgery (Hepatopancreatobiliary Surgery), The Affiliated Hospital of Southwest Medical University, Luzhou, 646000, People's Republic of China; [2]Academician (Expert) Workstation of Sichuan Province, Metabolic Hepatobiliary and Pancreatic Diseases Key Laboratory of Luzhou City, the Affiliated Hospital of Southwest Medical University, Luzhou, 646000, People's Republic of China; [3]Department of Oncology, the Affiliated Hospital of Southwest Medical University, Luzhou, Sichuan, 646000, People's Republic of China

*These authors contributed equally to this work

Correspondence: Shaozhi Fu; Xiaoli Yang, Email shaozhifu513@163.com; 344920646@qq.com

International Journal of Nanomedicine downloaded from https://www.dovepress.com/
For personal use only.

Objective: The combination of DOX and 5-Fu is an important chemotherapeutic regimen but lacks targeting to solid tumor sites. Precise drug delivery via folate-modified nanomaterials is an important measure to improve efficacy and reduce toxicity.

Methods: $CaCO_3$ nanoparticles served as the carrier for loading DOX and 5-Fu, followed by encapsulation with folic acid-modified polydopamine (PDA) to form a smart dual drug-carrying nanosystem called FA-DCFP. The nanoparticles (NPs) were characterized and the release kinetics and anti-tumor effectiveness of FA-DCFP were studied in vitro and in vivo.

Results: The prepared nanoparticles had an average particle size of 188.79±0.93nm and exhibited pH-sensitive drug release. Cellular experiments demonstrated that the synergistic effect of tumor cell calcium overload and chemotherapy resulted in tumor cell death. Small animal in vivo imaging showed that FA-DCFP was well enriched in the tumour region. In vivo experiments demonstrated that FA-DCFP exhibited significant inhibition of tumour growth, attenuation of toxic side effects, and good biosafety compared to other groups.

Conclusion: An intelligent-responsive nano-dual drug delivery system was developed to enhance the therapeutic effectiveness of tumors through calcium overload synergistic chemotherapy, offering a novel approach to tumor treatment.

Keywords: adriamycin, calcium overload, 5-fluorouracil, drug-targeting delivery, colon cancer

Introduction

Doxorubicin (DOX) and 5-fluorouracil (5-Fu) are widely used in combination therapy;[1,2] however, their lack of selectivity can lead to severe side effects, including cardiotoxicity, bone marrow suppression, and gastrointestinal reactions.[3–5] Therefore, enhancing the targeting capabilities of these chemotherapy drugs is essential for improving tumor efficacy and minimizing drug-related adverse effects.

Nanodrug delivery systems offer a promising solution to this challenge.[6,7] Innovative drug delivery platforms, such as nanoparticles,[8] nano hydrogels,[9] and nano microorganisms,[10] provide high drug loading capacity and suitable sizes, enabling the effective delivery of chemotherapy drugs to tumor sites through modifications of the nanodrugs. Bujalance Fernández designed a macroporous metal-organic framework for the loading and sequential release of 5-fluorouracil and doxorubicin.[11] Elaheh Ranjbar successfully encapsulated 5-fluorouracil 5-Fu and doxorubicin DOX in carboxymethyl starch and evaluated their co-delivery performance in vitro.[12] Xu utilized hierarchical mesoporous silica and albumin composite nanomaterials to deliver DOX and 5-fluorouracil, demonstrating inhibitory effects on tumor development in an in vivo hepatocellular carcinoma nude mouse model.[13]

Received: 1 April 2025
Accepted: 18 August 2025
Published: 23 August 2025

© 2025 Tang et al. This work is published and licensed by Dove Medical Press Limited. The full terms of this license are available at https://www.dovepress.com/terms.php and incorporate the Creative Commons Attribution – Non Commercial (unported, v4.0) License (http://creativecommons.org/licenses/by-nc/4.0/). By accessing the work you hereby accept the Terms. Non-commercial uses of the work are permitted without any further permission from Dove Medical Press Limited, provided the work is properly attributed. For permission for commercial use of this work, please see paragraphs 4.2 and 5 of our Terms (https://www.dovepress.com/terms.php).

Calcium carbonate ($CaCO_3$) nanoparticles have been identified as effective carriers for chemotherapy drug delivery.[14,15] The employment of calcium carbonate as a carrier for diverse drug delivery systems affords advantages including facile preparation, low cost, and stable nanoparticle morphology. Additionally, $CaCO_3$ nanomaterials can disrupt the calcium ion balance in the tumor microenvironment, leading to calcium overload and subsequent tumor cell death.[16,17] Their solubility in acidic environments aligns well with the acidic characteristics of tumors, facilitating the natural release of drugs within the tumor microenvironment.[18] This approach concurrently prevents disintegration under physiological conditions from causing damage to normal tissues.[19] These features establish $CaCO_3$ nanomaterials as intelligent drug carriers for precise delivery and effective release, thereby enhancing therapeutic efficacy while reducing systemic toxicity. Chang[20] and Hu[21] have demonstrated that $CaCO_3$-based carriers serve as effective therapeutic adjuvants in the treatment of colorectal cancer.

Drug-loaded nanoplatforms can exploit the Enhanced Permeability and Retention (EPR) effect to preferentially accumulate in tumor tissues during systemic circulation, thereby enabling sustained therapeutic efficacy.[22] Owing to the leakiness of tumor vasculature, nanoparticles can extravasate from the bloodstream through intercellular gaps in the endothelial lining and accumulate within tumor tissue. Concurrently, the dysfunctional lymphatic drainage in tumor tissues impedes effective clearance of extravasated therapeutic payloads, resulting in their prolonged retention within the interstitial space to potentiate sustained therapeutic outcomes.[23] But incorporating a targeting component can further improve the specificity of drug delivery systems.[24] A particularly promising approach involves utilizing the properties of folate receptors (FR). Folate receptors are glycoprotein membrane receptors located on the cell surface, playing a crucial role in the transport and metabolism of folate and its derivatives. The folate receptor family includes several subtypes, such as FR α, FR β, FR γ, and FR δ; among them, FR α (FOLR1) is primarily responsible for mediating intracellular folate transport. Through receptor-mediated endocytosis, FOLR1 enhances the internalization of folate to meet the growth and metabolic demands of cells.[25] Research has indicated that FOLR1 is highly expressed in various tumor cells, including colorectal cancer, hepatocellular carcinoma, and lung cancer, while exhibiting low or absent levels in normal cells.[26–28] This differential expression provides a strong foundation for the development of folate receptor-targeted drug delivery systems.[29,30]

In this study, as shown in Scheme 1, we designed an intelligent nano dual drug delivery system, FA-DCFP, incorporating $CaCO_3$ nanoparticles to encapsulate DOX and 5-Fu. These nanoparticles were coated with polydopamine (PDA) and subsequently modified with folic acid (FA). The drug-loaded nanoparticles are directed toward the tumor site through FA targeting. In the acidic tumor microenvironment, PDA and $CaCO_3$ nanoparticles gradually decompose, promoting the release of $CaCO_3$ and exerting anti-tumor effects alongside the chemotherapy drugs DOX and 5-Fu. Overall, these mechanisms work synergistically to enhance the therapeutic efficacy of the FA-DCFP system.

Materials and Methods

Materials

Anhydrous calcium chloride ($CaCl_2$), ammonium bicarbonate ($NH4HCO_3$), doxorubicin acid, dopamine hydrochloride, 5-fluorouracil, calcium-fluorescent probe, 1-ethyl-3-(dimethylamino)propylcarbodiimide (EDC) and N-hydroxysuccinimide (NHS) were purchased from Shanghai Maclean Co Ltd (Shanghai, China). Anhydrous ethanol and ammonia were purchased from Chengdu Kelong Chemical Co Ltd (Chengdu, China). MTT was purchased from Chengdu Kelong Chemical Co Ltd (Chengdu, China). Penicillin-streptomycin solution was purchased from Gibco (New York, USA).The AO fluorescent staining kit, alizarin red S staining solution (0.2%, pH 8.3), mitochondrial membrane potential kit (JC-1), and DAPI were purchased from Solbao Biotechnology Co Ltd (Beijing, China). The Fluo-4 calcium ion detection kit was purchased from Beyotime Biotechnology.

Cell Lines and Animals

The murine colorectal cancer cell line CT26, the human hepatocellular carcinoma cell line HepG2, and the human immortalized liver cell line THLE-2 were obtained from the Chinese Academy of Sciences Cell Bank and supplied by the Medical Laboratory Center of the Affiliated Hospital of Southwest Medical University. CT26 cells were cultured in 1640 medium containing 10% fetal bovine serum, penicillin (100 U/mL) and streptomycin (100 μg/mL), at 37°C in a 5%

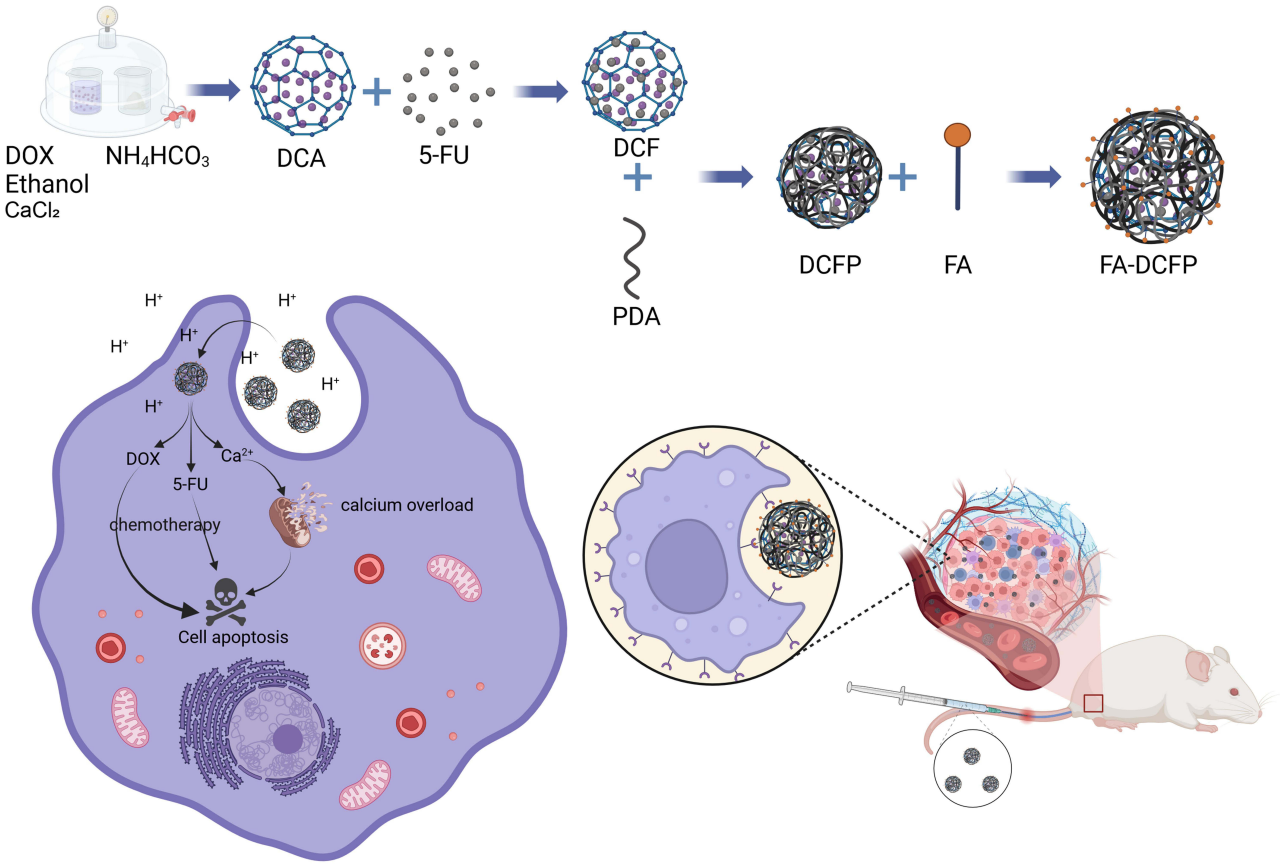

Scheme 1 Schematic illustration showing the fabrication process and antitumor mechanism of the FA-DCFP. Some abbreviations indicate as follows: $CaCO_3$, DCA ($CaCO_3$+DOX), DCF (DOX+$CaCO_3$+5-Fu), DCFP ($CaCO_3$+DOX+5-Fu+PDA) and FA-DCFP (FA+$CaCO_3$+DOX+5-Fu+PDA). *Created in BioRender. tang, y. (2025)* https://BioRender.com/i56v996.

CO_2 atmosphere. HepG2 and THLE-2 cells were cultured in DMEM containing 10% FBS, penicillin (100 U/mL) and streptomycin (100 μg/mL) at 37°C in a 5% CO_2 atmosphere.

Balb/c male mice were provided by Beijing Huafukang Biotechnology Co Ltd and housed on standard laboratory diet at an ambient temperature and humidity in air-conditioned chambers. All mice exhibited a state of well-being, with no instances of infections documented throughout the duration of the experiment. The use and handling of mice adhered to ethical guidelines outlined in the National Institutes of Health Guide for the Care and Use of Laboratory Animals. All experimental protocols involving animal subjects received approval from the Institutional Animal Care and Treatment Committee of Southwest Medical University (swmu20250011).

Synthesis of FA-DCFP

$CaCO_3$ nanoparticles were synthesized by the gas diffusion method, whereby 550 mg of anhydrous calcium chloride was added to 500 mL of anhydrous ethanol, which was then ultrasonically dissolved and set aside. A 100 mL volume of the prepared calcium chloride ethanol solution was transferred to a 100 mL beaker and covered with aluminium punched with small holes. Another small beaker was prepared and 5 g of dried ammonium bicarbonate was added, also covered with aluminium punched with small holes. Subsequently, the components were placed together in a vacuum drying oven. The reaction system was permitted to react in a vacuum environment at 40 °C for 24 hours. Following the reaction, the system was subjected to centrifugation at 12,000 rpm for 15 minutes, after which it was washed with anhydrous ethanol on two or three occasions. The process was then concluded with vacuum drying, resulting in the formation of $CaCO_3$ nanoparticles. The synthesis of $CaCO_3$ and DOX (DCA) was conducted via a one-pot method. The synthesis of $CaCO_3$ @DOX was performed in a similar manner to that of $CaCO_3$, with the exception that 5 mg of DOX was added to

a prepared calcium chloride ethanol solution (100 mL) and sonicated until fully dissolved. This solution was then placed in a vacuum drying oven for the reaction to proceed. The resulting product was $CaCO_3$@DOX nanoparticles. Following the reaction, the system was subjected to centrifugation at 12,000 rpm for 15 minutes, after which it was washed with anhydrous ethanol on two or three occasions.

A solution of 40 mg DCA in 80 mL anhydrous ethanol was prepared and dispersed evenly by ultrasonication. Subsequently, 5 mg 5-Fu in 20 mL anhydrous ethanol was added and ultrasonicated until completely dissolved. Finally, 20 mL of the 5-Fu solution was rapidly added to the DCA anhydrous ethanol solution under magnetic stirring at 800 rpm. The solution was stirred at room temperature for a period of 24 hours. Subsequently, the solution was transferred to a centrifuge tube and subjected to centrifugation at 12,000 rpm for 15 minutes. Thereafter, it was washed two or three times with anhydrous ethanol. Subsequently, the DCF ($CaCO_3$+DOX+5-Fu) nanoparticles were obtained through vacuum drying.

A solution of 5 mg DCF nanoparticles in 10 mL anhydrous ethanol should be prepared. Following ultrasonic dissolution, 150 μL of ammonia (1 M) and 1 mg of DA should be added to the round-bottomed flask, where they should react at 25 °C for 12 hours. The DCFP should be collected by centrifugation at 12,000 rpm for a period of 15 minutes. A quantity of 4 mg of DCFP should be added to 5 mL of anhydrous ethanol, and the solution should be mixed thoroughly by means of ultrasonication. The folic acid, EDC and NHS must be added to an appropriate quantity of anhydrous ethanol in a 1:1:1 ratio, and the mixture must be stirred for six hours under magnetic stirring at 600 rpm in order to activate the folic acid. The appropriate quantity of activated folic acid should then be added to the DCFP solution, and stirring should continue for a period of four hours. Subsequently, the precipitate should be collected by centrifugation at 12,000 rpm for 15 minutes. The precipitate should then be washed two or three times with anhydrous ethanol, and finally, the excess organic solvent should be evaporated using a rotary evaporator to obtain FA-DCFP nanoparticles.

Characterization of FA-DCFP

Particle size and polydispersity index (PDI) were determined by means of dynamic light scattering (DLS), repeat the measurement 3 times. Drug loading (DL) and encapsulation efficiency (EE) were quantified by UV spectrophotometry. The following equations were employed to calculate DL and EE. The conjugation efficiency of FA was determined using UV-Vis spectrophotometry.

$$\text{DOX drugloadingrate } (\%) = \frac{amount\ of\ \text{DOX}\ in\ \text{CaCO3}}{Quality\ of\ DCA\ after\ vacuumdrying} x100\%$$

$$5-\text{Fu drugloadingrate } (\%) = \frac{amount\ \ of\ 5-\text{FU}\ in\ \text{DCA}}{Quality\ \ of DCF\ after\ vacuumdrying} x100\%$$

The successful synthesis of FA-DCFP nanoparticles was corroborated through the utilisation of transmission electron microscopy (TEM), X-ray photoelectron spectroscopy (XPS), X-ray diffraction (XRD) and Fourier transform infrared spectroscopy (FTIR).

In vitro Drug Release of FA-DCFP

The release of 5-Fu and DOX from FA-DCFP was performed at pH 5.5, 6.5 and 7.4 using dialysis method. Briefly, the FA-DCFP solution (DOX and 5-Fu equivalent of 1 mg and 0.68 mg, respectively) was placed in a dialysis bag (MWCO 8000 Da) and immersed into 50 mL of PBS solution with different pH value. 2.0 mL of the external buffer was collected and replaced by a fresh buffer at predetermined time point. The concentration of DOX and 5-Fu was determined using ultraviolet spectrophotometry. This experiment was repeated three times.

The release kinetics of DOX and 5-Fu from FA-DCFP using first-order, Higuchi, and Korsmeyer-Peppas models. The release curves were fitted using Python, and the coefficient of determination R^2 was calculated to select the best-fitting model.

In vitro Cytotoxicity

The CT26 and HepG2 cells were inoculated into 96-well culture plates at a density of 5000 cells per well and maintained in culture for 24 hours. Subsequently, the original medium was removed and replaced with serum-free medium

containing different concentration gradients of DOX, 5-Fu, $CaCO_3$, DCA, FCA, and FA-DCFP, and the culture was continued for 24 hours, the drug concentration gradient of FA-DCFP was 400 μg/mL, 200 μg/mL, 100 μg/mL, 50 μg/mL, 25 μg/mL, and 12.5 μg/mL, with 100 μL of the corresponding drug added to each well. Subsequently, 20 μL of MTT solution, with a concentration of 5 mg/mL, was added to each well and the plates were incubated for a further 4 to 6 hours. At the conclusion of the incubation period, 150 μL of dimethyl sulfoxide (DMSO) was added to each well, and the absorbance was measured at 490 nm using a FLUOstar Omega enzyme marker. Repeat the experiment three times.

The CT26 cell line was inoculated in 6-well culture plates at a density of 1.0×10^5 cells per well in conjunction with HepG2 cells. The plates were then incubated in a cell incubator for a period of 24 hours. Subsequently, the original medium was replaced with fresh medium containing DOX, 5-Fu, $CaCO_3$, DCA, FCA and FA-DCFP, and the incubation was continued for 24 hours, the drug used was equivalent to 50 μg/mL DOX, with a total volume of 2 mL. Subsequently, the cells were subjected to a dual staining procedure utilising Calcein-AM (at a concentration of 1 μg/mL) and PI (also at a concentration of 1 μg/mL) for a period of 30 minutes. Subsequently, the stained cells were observed and analysed using an inverted fluorescence microscope.

In vitro Cell Migration Assays

The inhibitory effect of FA-DCFP on the migration of CT26 with HepG2 cells was evaluated through the utilisation of a scratch healing assay. Initially, the cells were evenly distributed in a 6-well plate, after which scratches were made on the cell layer using a sterile needle. Subsequently, the cells were gently washed three times with culture medium to remove cellular debris resulting from the scratches. Subsequently, the medium was supplemented with DOX, 5-Fu, $CaCO_3$, DCA, FCA, and FA-DCFP at an equivalent DOX concentration of 5 μg/mL (2mL), and the plates were incubated. The cells were observed and imaged at three time points (0 h, 12 h and 24 h) after treatment using a light microscope to assess the migration and scratch healing of the cells under different drug treatments.

In vitro Cellular Uptake

The CT26 and HepG2 cells were inoculated in 6-well culture plates at a density of 1.0×10^5 cells per well. Once the cells had successfully attached to the wall, the DOX, DCA, FA-DCFP and FA+FA-DCFP solutions, which had been dispersed in the medium, were added to the culture system. The equivalent concentration of DOX was 5 μg/mL (2mL), and the cells were incubated with the solutions for a period of six hours. Subsequently, the culture system was treated with a DAPI solution for the purpose of nuclear staining of the cells, after which incubation was continued. Subsequently, the culture substrate was removed and observed under an inverted fluorescence microscope, with the results duly recorded. THLE-2 cells were used as normal controls and subjected to the same treatment to evaluate the selectivity of FA-DCFP toward tumor cells.

Intracellular Ca^{2+} Detection

The CT26 and HepG2 cell lines were seeded at a density of 1.0×10^5 cells per well in a 6-well plate. Once the cells had successfully adhered to the wall, the culture system was treated with $CaCO_3$, FCA, DCA, FA-DCFP and FA + FA-DCFP (50 μg/mL, 1 mL) solution for a period of 4 hours. Subsequently, Fluo-4 AM was added and incubated for 1 hour to stain the cells, followed by three washes with PBS. Finally, the cells were observed under an inverted fluorescence microscope and the results were recorded.

In vitro Cell Calcification Test

CT26 and HepG2 cells were inoculated in 6-well culture plates at a cell density of 1.0×10^5 per well. Once the cells had successfully attached to the wall, the medium was removed and 2 mL of FA-DCFP (25 μg/mL, 2 mL) solution was added at 3 h, 6 h, 12 h and 24 h time points, respectively. Following the removal of the medium and fixation of the cells with 95% ethanol, the cells were stained with 2 mL of alizarin red dispersed in Tris buffer (0.2%, pH 8.3) for 30 minutes, after which they were observed. Repeat the experiment three times.

Mitochondrial Integrity Assays

A suspension of CT26 cells was inoculated in 6-well culture plates at a density of 1.0×10^5 cells per well. Following successful wall application of the cells, the plates were treated with FA-DCFP (100 μg/mL, 2 mL) nanomedicine for 24 hours. At the conclusion of the treatment period, any residual nanomedicine was removed. The JC1 solution was then added to the cells and allowed to incubate for 30 minutes, during which time the final results of the experiment were observed and recorded.

Blood Compatibility Analysis

The FA-DCFP was dissolved in NS to create a solution of 2 mg/mL, 1 mg/mL, 0.5 mg/mL and 0.25 mg/mL. One millilitre of the various concentrations of FA-DCFP was combined with one millilitre of an erythrocyte suspension (0.2%, V/V), and incubated at 37°C for four hours. The positive control was a double-steamer, while saline served as the negative control. The optical density (OD) value was determined by ultraviolet (UV) spectrophotometry, with a measurement range of 414 nanometres (nm).

In vivo Imaging Study

Use of ICG-labeled nanoparticles for in vivo fluorescence imaging analysis. To synthesize indocyanine green ICG-labeled nanoparticles, ICG (5 mg) was added to 5 mL of FA-DCFP solution (1 mg/mL) and stirred in the dark for 24 h at room temperature. FA-DCFP was then collected by centrifugation. 100 μL of ICG or FA-DCFP/ICG (equivalent to 1 mg/kg of ICG) was injected into the tail vein of the mice when the tumor reached about 200 mm^3, and the mice were fluorescently imaged at 12, 24, and 48 hours after the injection of the drug.

In vivo Antitumor Efficacy

The CT26 tumour model was established by subcutaneously injecting 5×10^6 CT26 cells and 100 μL RPMI-1640 liquid medium into the right leg of male Balb/c mice until the tumour volume reached 75–100 mm^3. The mice were randomly divided into six groups, with each group comprising 10 mice. The mice were treated differently according to the following conditions: Group I served as the positive group, while Groups II, III, IV, V, and VI were treated with Free 5-Fu, Free DOX, FCA, DCA, and FA-DCFP, respectively. Each group of mice was administered an intravenous injection of the respective preparation (0.1 mL, calculated as 5 mg/kg of free DOX) every other day. The injections were repeated on three occasions, and the mice's tumour size and body weight were measured at two-day intervals. Tumour volume was calculated according to the following formula: Tumour volume (V) was calculated using the formula $V = 1/2 \times AB,^2$ where V is the tumour volume in mm^3, A is the long diameter of the tumour in mm, and B is the short diameter of the tumour in mm.Mice were executed on day 14 after initiation of treatment, and tumor tissues were collected and subjected to hematoxylin and eosin (H&E), TUNEL staining, and Ki-67 examination to assess the therapeutic effect of the drugs on the tumors.

Toxicity Analysis by Organ

To evaluate the biosafety of the nanomedicine, euthanasia procedures were conducted on all mice on the 15th day following the conclusion of the treatment period. Subsequently, the five key organs of the mice, namely the heart, liver, spleen, lungs and kidneys, were harvested and subjected to H&E staining analysis. Furthermore, Masson staining of heart tissues was conducted to gain deeper insights into the fibrosis of myocardial tissues. The objective of these initiatives was to comprehensively assess the potential effects that nanomedicines may have on various organs.

Routine Blood and Biochemical Analysis

In order to gain a deeper understanding of the toxicity characteristics of FA-DCFP in vivo, we selected healthy Kunming white mice as the experimental subjects. The negative control group was given saline (NS), while the FA-DCFP experimental group was administered the drug at an equivalent dose of DOX 5 mg/kg by intravenous injection at a frequency of every other day for a total of three injections. On the fourteenth day of the experiment, blood samples were collected from the mice using the retro-orbital venous plexus method. Subsequently, biochemical analyses and routine blood tests were conducted on the aforementioned blood samples.

Statistical Analysis

Statistical analysis All experiments were conducted at least in triplicate; data were expressed as mean ± standard deviation (SD). The quantitative data were presented as mean ± standard deviation (SD), and statistical significance between groups was analyzed using an unpaired Student's *t*-test. A p-value of less than 0.05 was considered statistically significant.

Results

Characterization of FA-DCFP

Transmission electron microscopy (TEM) results showed that both $CaCO_3$ nanoparticles and FA-DCFP nanoparticles exhibited uniform spherical shape and good dispersion, indicating that the synthesized nanoparticles were uniformly sized and well dispersed (Figure 1A(a) and A(b)). The mean particle size of the $CaCO_3$, DCA ($CaCO_3$+DOX), DCF ($CaCO_3$+DOX+5-Fu), DCFP ($CaCO_3$+DOX+5-Fu+PDA), and FA-DCFP ($CaCO_3$+DOX+5-Fu+PDA+FA) nanoparticles

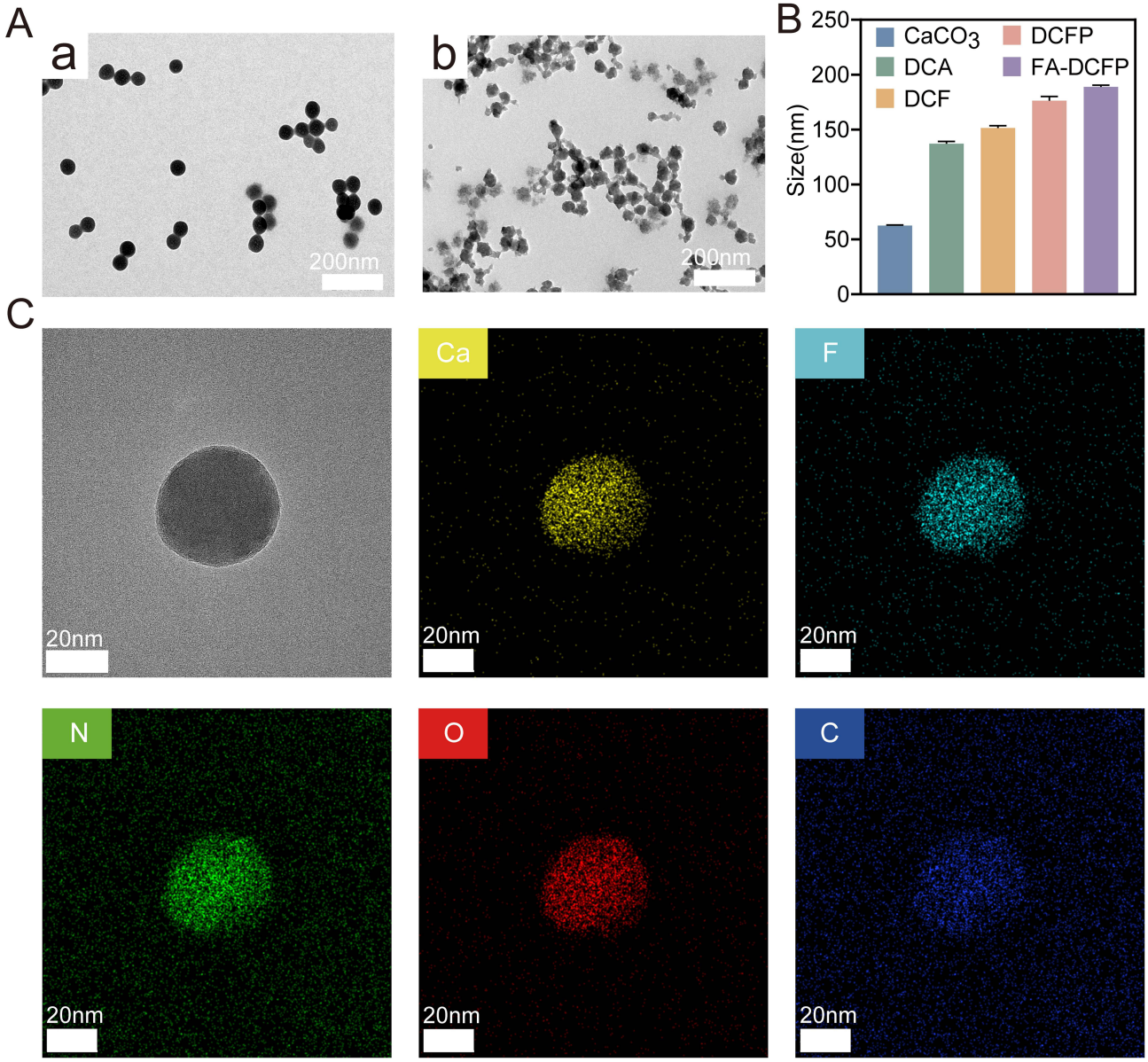

Figure 1 In vitro characterization of $CaCO_3$ and FA-DCFP. (**A**) TEM images of (**a**) $CaCO_3$ nanoparticles, (**b**) FA-DCFP nanoparticles. (**B**) Average particle size (n = 3) of $CaCO_3$, DCA ($CaCO_3$+DOX), DCF (DOX+$CaCO_3$+5-Fu), DCFP ($CaCO_3$+DOX+5-Fu+PDA) and FA-DCFP (FA+$CaCO_3$+DOX+5-Fu+PDA). (**C**) High–angle annular dark–field scanning transmission electron microscope (HAADF-STEM) image and elemental mapping of the FA-DCFP nanoparticles.

https://doi.org/10.2147/IJN.S523621

was found to be 62.50±0.58nm, 137.11±2.03nm, 151.40±2.07nm, 176.22±3.91nm, and 188.79±1.61nm, respectively (Figure 1B). The PDI of $CaCO_3$ was 0.18±0.01, DCA was 0.14±0.03, DCF was 0.16±0.03, DCFP was 0.25±0.01, and FA-DCFP was 0.25±0.01 (Figure S1). The results showed that the zeta potential of nano $CaCO_3$ was 7.64±0.57 mV, DCA was 9.82±0.40 mV, and DCF was 11.27±0.31 mV. After coating with polydopamine, the overall zeta potential of the nanoparticles became negative, with DCFP measuring −15.77±1.14 mV. Upon further modification with folic acid, the zeta potential decreased even more, with FA-DCFP showing a value of −21.93±0.35 mV (Figure S2). Elemental mapping confirmed the presence of Ca and F in the FA-DCFP NPs (Figure 1C). The drug loading rate of DOX in FA-DCFP was determined to be 11.06±0.49%, with an encapsulation rate of 91.37±0.16%. The drug loading rate of 5-Fu in FA-DCFP was determined to be 7.89±0.15%, with an encapsulation rate of 64.68±1.41%. The elemental energy spectrum demonstrated the presence of calcium and fluorine in the FA-DCFP nanoparticles.

The X-ray diffraction (XRD) pattern (Figure 2A) of FA-DCFP exhibits characteristic peaks at 24.8°, 27.0°, and 32.7°, which show significant overlap with the simulated standard $CaCO_3$ peaks. To further verify the composition of the nanomaterials and the distribution of each element, we employed X-ray photoelectron spectroscopy (XPS) to analyze the constituent elements of FA-DCFP. The results indicate that FA-DCFP comprises five elements: Ca, C, N, F, and O, which are uniformly distributed within the nanoparticles (Figure 2B). Furthermore, Figure 2C illustrates two distinct Ca 2p characteristic peaks at 346.67 eV and 350.08 eV. The emergence of these peaks unequivocally confirms that the Ca element exists in the material as Ca^{2+} ions. Additionally, the distinct F peak observed in Figure 2D appears at 687.25 eV, providing insights into the chemical state of the F element in FA-DCFP. The FTIR spectra of pure folic acid and FA-DCFP are presented in Figure 2E. The FTIR spectrum of FA-DCFP reveals an absorption peak at 2907.03 cm^{-1} compared to pure folic acid, which can be attributed to the -CH bond stretching vibrations of folic acid. Moreover, the FTIR spectrum of FA-DCFP exhibits absorption peaks at 1633.54 cm^{-1} and 1408.75 cm^{-1}, likely corresponding to the aromatic ring stretching of the pteridine skeleton and the p-amino benzoic acid moieties of folic acid, By comparing the absorbance before and after the reaction, the conjugation efficiency of FA was calculated. The results showed that the conjugation efficiency of FA to the nanoparticles was 57.23±2.17% (Figure S3). In summary, the experimental results not only validate the presence of the $CaCO_3$ structure within the FA-DCFP material but also provide comprehensive support for the successful formation of FA-DCFP.

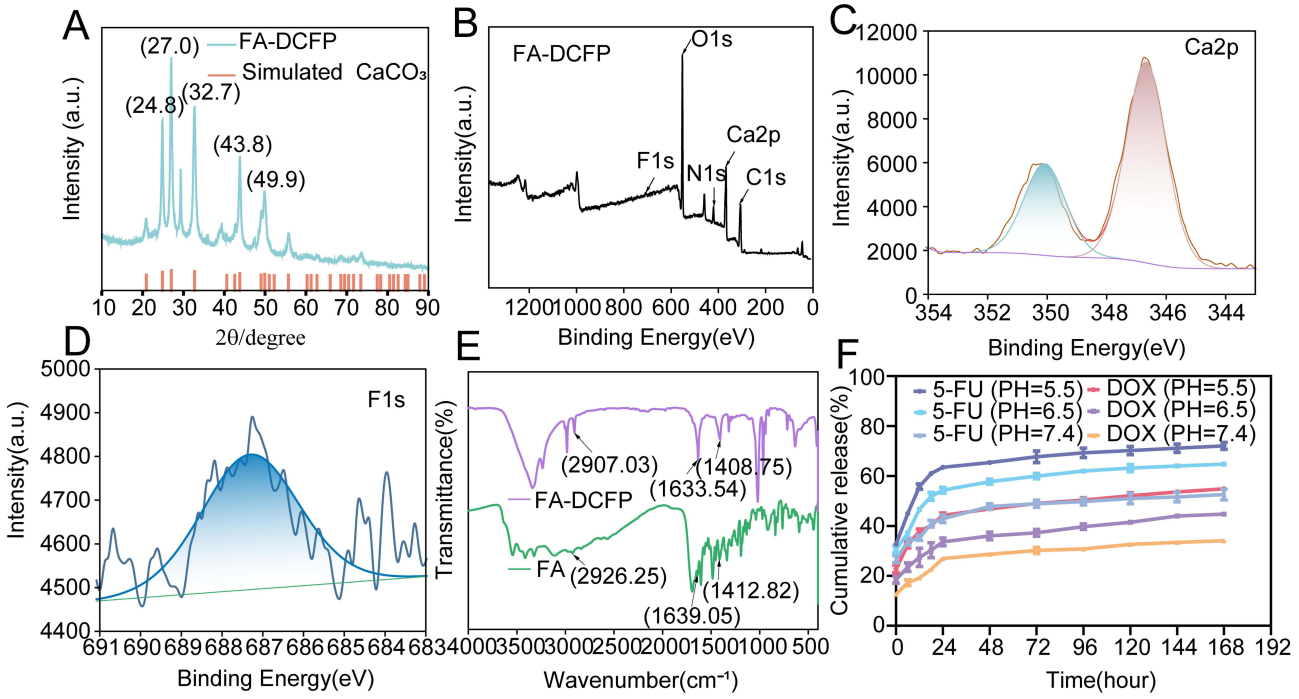

Figure 2 In vitro characterization of FA-DCFP. (**A**) XRD patterns of the FA-DCFP nanoparticles. (**B**) XPS spectrum of the FA-DCFP nanoparticles. (**C**) XPS spectrum of Ca 2p in the FA-DCFP nanoparticles. (**D**) XPS spectrum of F 1S in the FA-DCFP nanoparticles. (**E**) Fourier transform infrared (FTIR) spectra of folic acid and FA-DCFP. (**F**) In vitro release profiles of FA-DCFP in PBS at pH 5.5, 6.5, and 7.4 (n = 3, mean ± SD).

In vitro Drug Release of FA-DCFP

Figure 2F illustrates the typical drug release profiles of FA-DCFP at three distinct pH values. The release of both DOX and 5-Fu is pH-dependent, with a more rapid release observed at pH 5.5 compared to pH 6.5 and 7.4. Notably, the release of 5-Fu occurs significantly faster than that of DOX. By comparing the drug release behavior of FA-DCFP with that of free 5-Fu and free DOX (Figure S4), and fitting the release profiles to established mathematical models (Table 1), it was demonstrated that the drug release from FA-DCFP follows Fickian diffusion, exhibiting a sustained release pattern. Additionally, the study reveals that FA-DCFP exhibits remarkable responsive characteristics in acidic environments.

In vitro Cytotoxicity

CT26 cells demonstrated a significantly higher uptake of FA-DCFP nanoparticles (NPs) compared to free DOX. The addition of folic acid led to a notable reduction in cellular uptake, suggesting that the drug facilitates internalization by binding to folate receptors on tumor cells (Figure 3A). A similar uptake pattern was observed in HepG2 cells (Figure S5). THLE-2 cells were used as non-tumor control cells, and no significant differences in drug uptake were observed among the treatment groups in these normal cells (Figure S6). To evaluate the in vitro cytotoxicity of $CaCO_3$ on CT26 cells, the survival rate gradually declined with increasing calcium concentration, indicating that $CaCO_3$ exerts a certain degree of cytotoxicity against tumor cells (Figure 3B). Specifically, the survival rates in the DCA and free DOX groups decreased from 75.21±2.80% to 25.99±2.19% and from 95.35±0.29% to 30.36±1.10%, respectively. Similarly, the survival rates in the FCA and free 5-Fu groups reduced from 70.82±6.32% to 38.16±1.74% and from 73.81±2.07% to 54.76±3.53%. Notably, the survival rate of the FA-DCFP group dramatically decreased from 50.21±1.02% to 19.18±0.84% as the concentration increased, which was significantly greater than that of the other groups. This clearly indicates that the FA-DCFP nanocomposites possess superior efficacy in inhibiting tumor cell growth compared to any single drug. Additionally, a comparable trend in cytotoxicity was observed in the HepG2 cell system (Figure S7). Scratch assays demonstrated that all NPs inhibited the migration of CT26 cells compared to the controls (Figure 3C and D), with a similar effect noted in HepG2 cells (Figures S8 and S9). The toxic effects of different drug formulations on CT26 (Figure 3E) and HepG2 (Figure S10) cells were assessed using calcein-AM/propidium iodide (PI) live/dead cell staining. The control group showed no cell death (indicated by red staining). $CaCO_3$ caused a modest level of cell death, while the FCA and DCA groups demonstrated a higher proportion of cell death compared to the free drug group. The FA-DCFP group exhibited the highest degree of cytotoxicity. In conclusion, FA-DCFP can be selectively internalized by tumor cells, inhibit tumor cell migration, and induce tumor cell death.

Table 1 Correlation Coefficient (R^2) Values According to First-Order, Higuchi, and Korsmeyer–Peppas and Related Kinetic Constants

Sample	Mathematical Model	Kinetic Constants	R^2
FA-DCFP (5-Fu, PH=5.5)	First-order: $\frac{Mt}{M0} = e^{-k1t}$	k_1=0.24±0.02	0.66 ±0.01
	Higuchi model: $\frac{Mt}{M0} = K_H\sqrt{t}$	K_H=2.64±0.12	0.76 ±0.01
	Korsmeyer-Peppas model: $\frac{Mt}{M0} = kt^n$	k=1.96±0.01 n=0.13±0.01	0.92 ±0.01
FA-DCFP (DOX, PH=5.5)	First-order: $\frac{Mt}{M0} = e^{-k1t}$	k_1=0.17±0.02	0.61 ±0.06
	Higuchi model: $\frac{Mt}{M0} = K_H\sqrt{t}$	K_H=2.28±0.05	0.88 ±0.01
	Korsmeyer-Peppas model: $\frac{Mt}{M0} = kt^n$	k=0.46±0.02 n=0.15±0.01	0.98 ±0.01

https://doi.org/10.2147/IJN.S523621

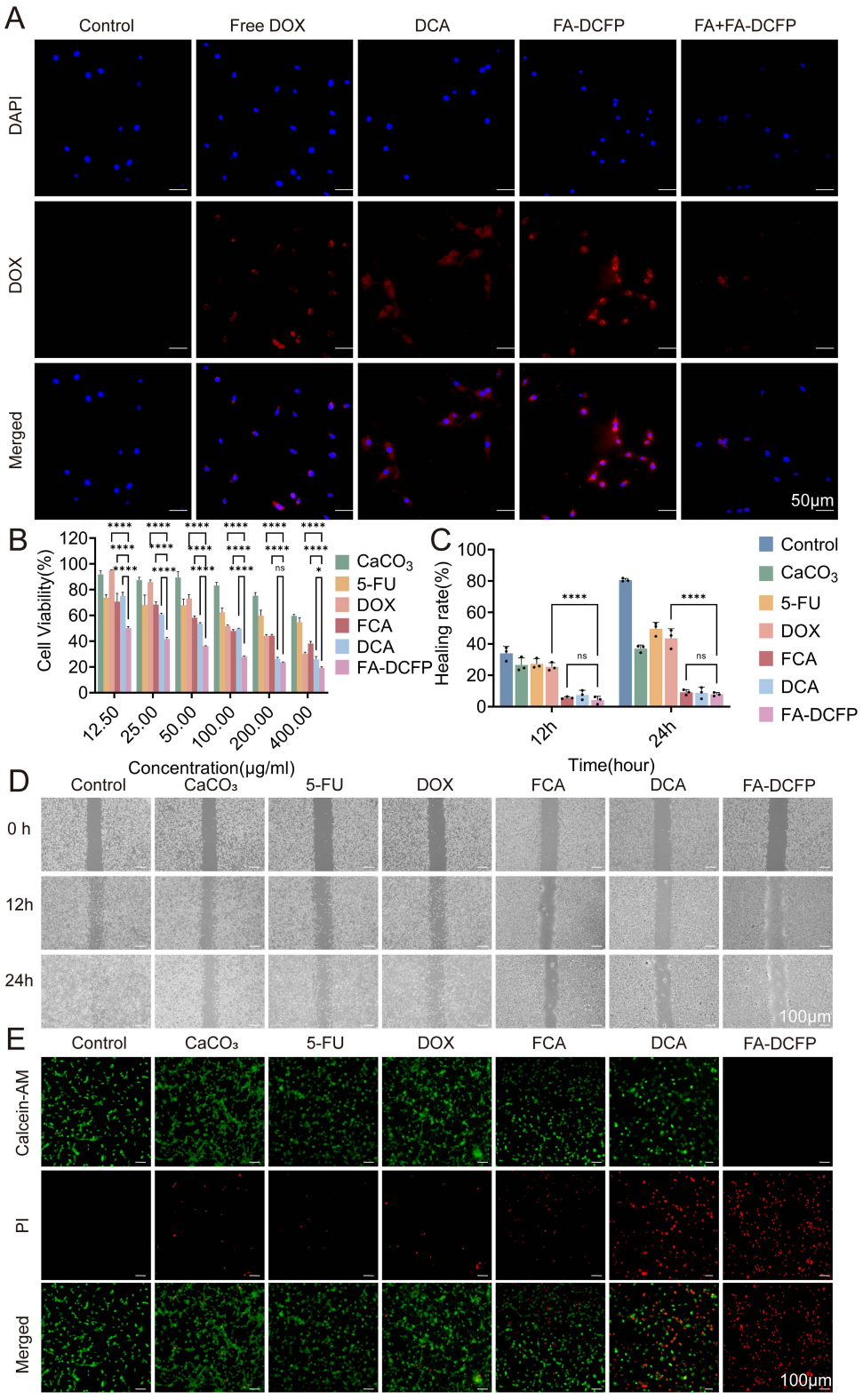

Figure 3 In vitro cell experiments. (**A**) Fluorescence images of different drugs taken up by CT26 cells. (**B**) Cell viability of the $CaCO_3$, 5-Fu, DOX, FCA, DCA and FA-DCFP nanoparticles on CT26 cells. (**C**) Healing rate of each group. (**D**) Photographs of wound healing taken at 0, 12, and 24 h. (**E**) Live/dead staining of CT26 cells treated with various drugs for 24 h: calcein-AM (green, live cells), PI (red, dead cells). Some abbreviations indicate as follows: FCA ($CaCO_3$+5-Fu); DCA ($CaCO_3$+DOX); FA-DCFP (FA+$CaCO_3$+DOX+5-Fu+PDA). Results are presented as means±SD. ns: no statistical significance, **P*<0.05, *****P*<0.0001.

FA-DCFP Induces Tumour Cell Death by Promoting Mitochondrial Dysfunction and Calcium Overloading

To evaluate intracellular Ca^{2+} uptake by tumor cells using different nanoparticles (NPs), we employed Fura-4 AM calcium fluorescence, which emits green fluorescence upon binding to Ca^{2+}. Figure 4A demonstrates that the control group exhibited minimal green fluorescence, the $CaCO_3$ group had a slight increase, while the FA-DCFP group displayed a significant enhancement in green fluorescence, which decreased with the addition of folic acid; similar uptake was observed in HepG2 cells (Figure S11). Furthermore, Alizarin Red S formed an orange-red complex with calcium ions, revealing that the areas of staining in FA-DCFP-treated cells increased over time, with calcification nearly complete after 24 hours (Figure 4B); similar uptake was observed in HepG2 cells (Figure S12). To investigate the mechanism of FA-DCFP-induced tumor cell death, we measured mitochondrial membrane potential (MMP) integrity using the JC-1 probe, which emits red fluorescence at intact MMP and transitions to green fluorescence upon depolarization. As shown in Figure 4C, tumor cells treated with FA-DCFP exhibited a pronounced green fluorescence signal, indicating a reduction in MMP; similar uptake was observed in HepG2 cells (Figure S13). This suggests that FA-DCFP significantly enhances intracellular Ca^{2+} uptake in tumor cells, leading to increased calcification and decreased mitochondrial membrane potential, which may contribute to its cytotoxic effects.

In vivo Imaging Study

Indo-cyanine green(ICG)-labeled FA-DCFP was administered intravenously to visualize the biodistribution in vivo. While free ICG was observed to be gradually cleared over time, FA-DCFP/ICG was found to accumulate in tumour tissue 48 hours after injection, thereby confirming the active targeting ability of FA-DCFP (Figure 5A). Additionally, ex vivo imaging of the tumour tissue after 48 hours demonstrated a notable fluorescent signal (Figure 5B).

In vivo Antitumor Efficacy

As shown in Figure 6A, the FA-DCFP group exhibited the smallest tumors along with the slowest tumor growth rate compared to the other groups (Figure 6B–D). By day 14, tumor growth in the FA-DCFP group was significantly inhibited (Figure 6E). In contrast, most mice in the free 5-Fu and free DOX groups displayed symptoms such as emaciation and poor mental status, which were attributed to the toxic side effects of the free chemotherapeutic agents. Notably, no significant weight loss was observed in mice from the other treatment groups (Figure 6F). The FA-DCFP treatment also resulted in a higher percentage of TUNEL-positive apoptotic cells within the tumor tissues (Figure 6G), indicating an enhanced anti-tumor effect. TUNEL staining revealed a significantly greater percentage of positive cells in the FA-DCFP

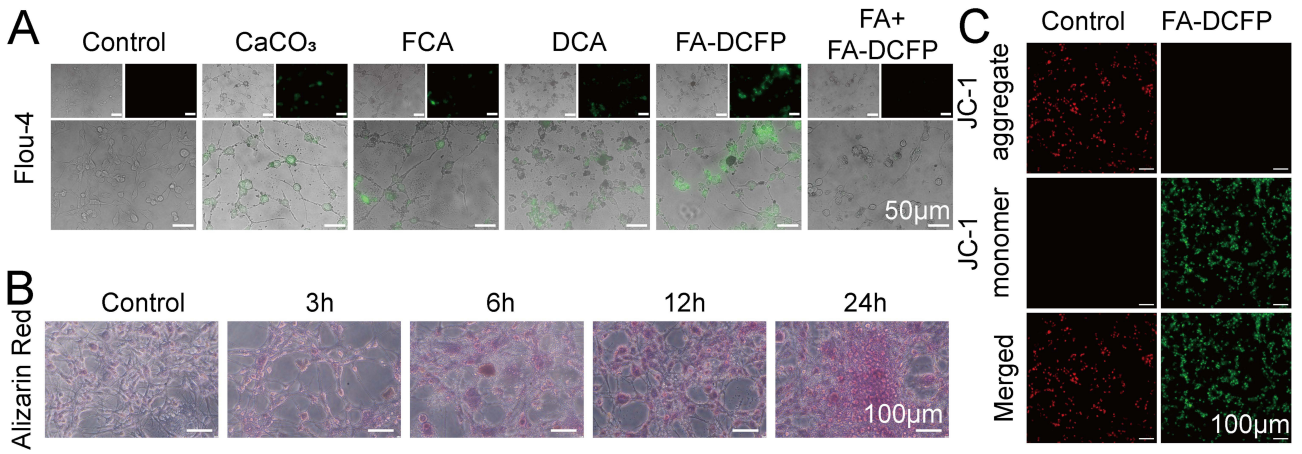

Figure 4 In vitro biochemical characterizations. (**A**) Fluorescence image of $CaCO_3$, FCA ($CaCO_3$+5-Fu), DCA ($CaCO_3$+DOX), FA-DCFP (FA+$CaCO_3$+DOX+5-Fu+PDA) and FA+FA-DCFP treated tumour cells for 24 hours and then stained with Flou-4 (n = 3). (**B**) Tumor cells were incubated with FA-DCFP for varying periods and then stained with alizarin red to identify in vitro cellular products that exhibited red areas of calcification (n = 3). (**C**) Tumour cells were incubated with FA-DCFP for 24 hours, and then stained with JC-1 (n = 3).

https://doi.org/10.2147/IJN.S523621

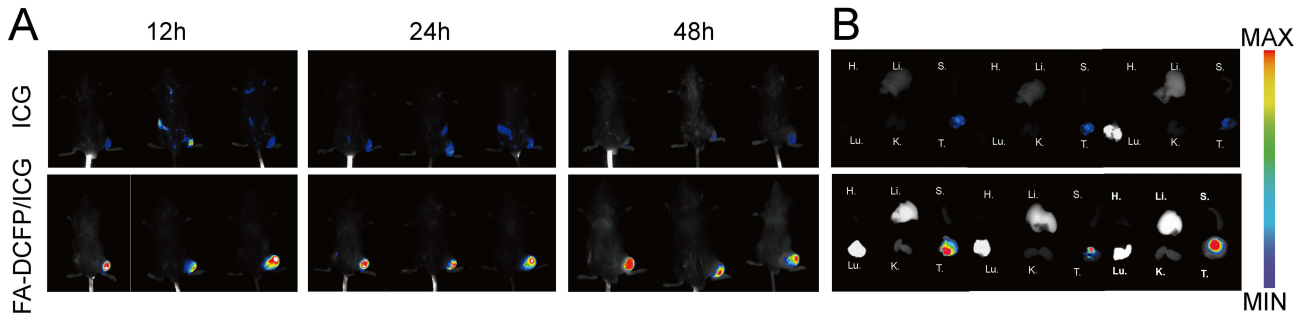

Figure 5 In vivo evaluation of drug distribution. (**A**) Fluorescence images of CT26 tumor-bearing mice after intravenous injection of free ICG, FA-DCFP/ICG. (**B**) In vitro fluorescence images of isolated organs and tumors at 48 h of postinjection (H: heart, Li: liver; (S) spleen; Lu: lung, (K) kidney, (T) tumor).

group compared to the other groups (Figure 6H). Furthermore, the FA-DCFP treatment demonstrated a marked inhibitory effect on tumor cell proliferation, as evidenced by immunohistochemical analysis using HE and Ki-67 staining, with the lowest percentage of Ki-67-positive cells observed in the FA-DCFP group (Figure 6I). In summary, the findings suggest that FA-DCFP treatment is effective in inhibiting tumor growth and promoting apoptosis.

Biocompatibility Assessment

H&E staining showed that no obvious signs of tissue damage were observed in the heart, liver, spleen, lungs and kidneys in any of the groups (Figure 7A), and no signs of myocardial fibrosis were observed in the Masson staining images in any of the groups (Figure 7B). Haemolysis test proves FA-DCFP is safe for red blood cells (Figure S14). Finally, hematological parameters were also normal in all groups, indicating no significant toxic effects of FA-DCFP compared to the control group (Figure 7C).

Discussion

The acidic microenvironment of tumors plays a significant role in promoting tumor growth, metastasis, angiogenesis, and inhibiting immune cell functions.[31,32] The unique characteristics of this microenvironment can be utilized to develop targeted therapies for tumors.[33–35] In the present study, calcium carbonate nanoparticles serve as acid-responsive drug delivery vehicles that intrinsically exploit the EPR effect to accumulate within solid tumor sites.

While it is feasible to target tumors by leveraging their acidic microenvironment, there is often a lack of specificity in tumor recognition. Many tumor cells exhibit high expression levels of specific receptors on their surfaces, making the receptor-ligand interaction a viable approach for selectively targeting drugs to tumor tissues.[36,37] Xu successfully developed dual phototherapy techniques by constructing integrin αvβ3 receptor-targeted nanomicelles (NanoDTPA-S/RGD).[38] Similarly, Kang utilized hyaluronic acid (HA) to target the tumor-specific receptor CD44, delivering chemotherapy agents and photothermal agents directly to the tumor site.[39] Liu created a non-G-quadruplex DNA aptamer for nucleolin (NCL), which is used for both diagnosis and treatment of bladder cancer.[40] These studies illustrate how leveraging specific receptors on tumor cell surfaces can enhance targeted anti-tumor therapy and diagnostic accuracy. The targeted anti-tumor nanoplatforms that employ the ligand-receptor mechanism for delivering chemotherapy drugs not only effectively reduce the systemic toxic side effects of these medications but also preserve their anti-tumor efficacy against tumor tissues.

Given the overexpression of folate receptors in certain tumors, considerable efforts have focused on utilizing these receptors as targets for cancer diagnosis, treatment, and the development of nanodrugs.[26,41] Yuan developed a nanoregulator that uses a core of hemoglobin (Hb) and iron ions (Fe^{3+}) conjugated with PDA, surrounded by glucose oxidase, with folate-targeting capabilities to synergistically regulate the tumor microenvironment.[42] Wei designed a glutathione (GSH) depleting, virus-like silica nanoprobe with a Gd coating and FA modification to enhance the radiosensitivity of breast cancer patients.[43] Folate molecules utilized in this study have previously demonstrated effective targeting in colon cancer.[28,44] In our in vitro experiments, folate receptor FR-targeted nanoparticles FA−DCFP demonstrated significantly enhanced cellular uptake in colorectal carcinoma cells CT26 compared to free drug controls, attributable to FR overexpression on the cell surface. This targeted uptake was competitively inhibited by free folate

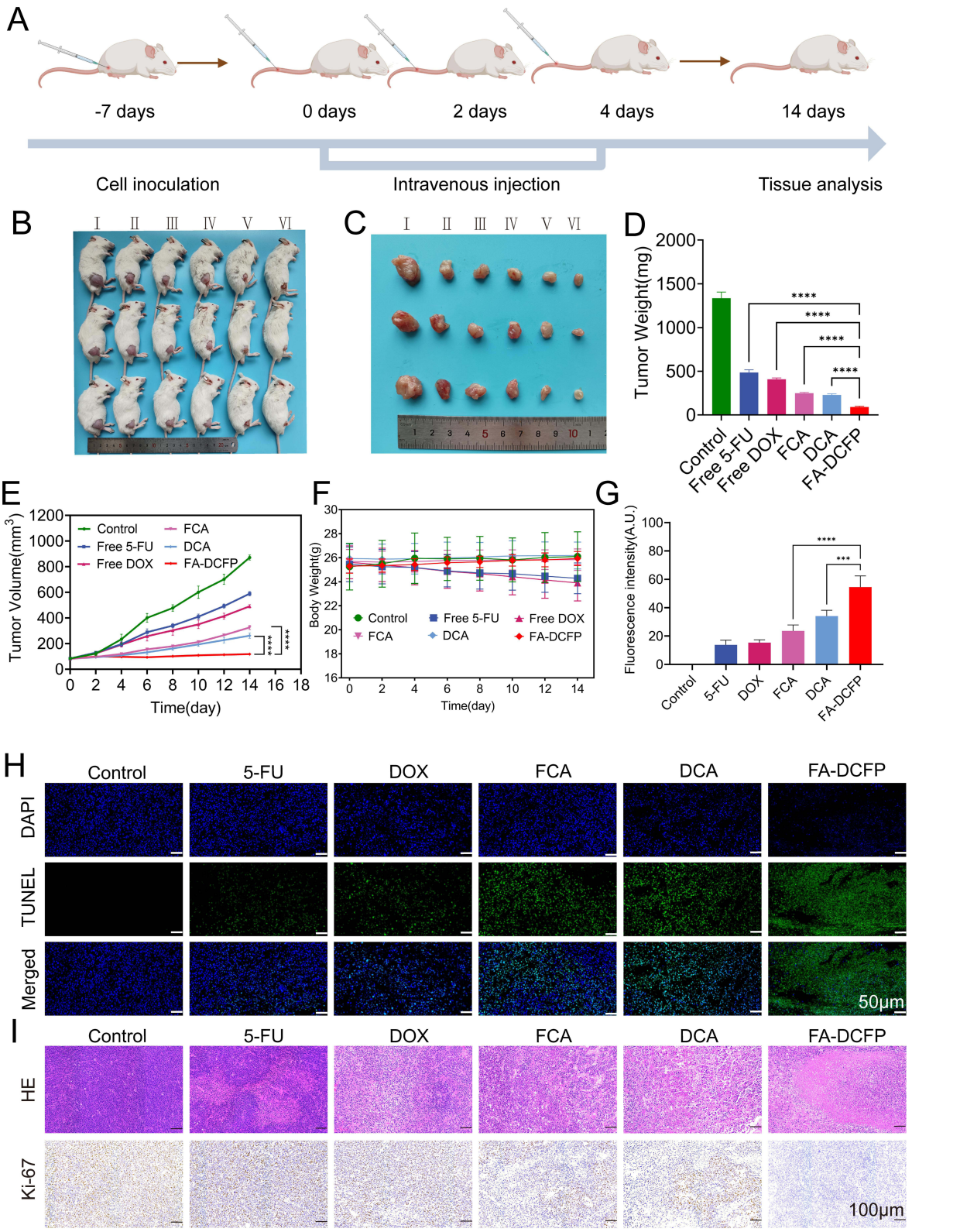

Figure 6 In vivo evaluation of antitumor efficacy. (**A**) A schematic diagram of the treatment procedure. (**B**) Representative photographs of CT26 tumor bearing mice were taken on day 14 after treatments (n = 3), (I: Control, II: 5-Fu, III: DOX, IV: FCA ($CaCO_3$+5-Fu), (V) DCA ($CaCO_3$+DOX), VI: FA-DCFP (FA+$CaCO_3$+DOX+5-Fu+PDA)). (**C**) Representative photographs of isolated tumors (n = 3). (**D**) Weight of tumors. (**E**) Change in tumor volume (n = 6). (**F**) Body weight fluctuations during treatment (n = 6). (**G**) The quantitative fluorescence intensity of tumor tissue was analyzed by TUNEL in each group. (**H**) Apoptosis of tumor tissue stained with DAPI (blue) and TdT–mediated dUTP nick–end labeling(TUNEL) (green) on day 15 of treatment. (**I**) Immunohistochemical staining of H&E and Ki-67. Results are presented as means±SD. ***P<0.001, ****P<0.0001.

https://doi.org/10.2147/IJN.S523621

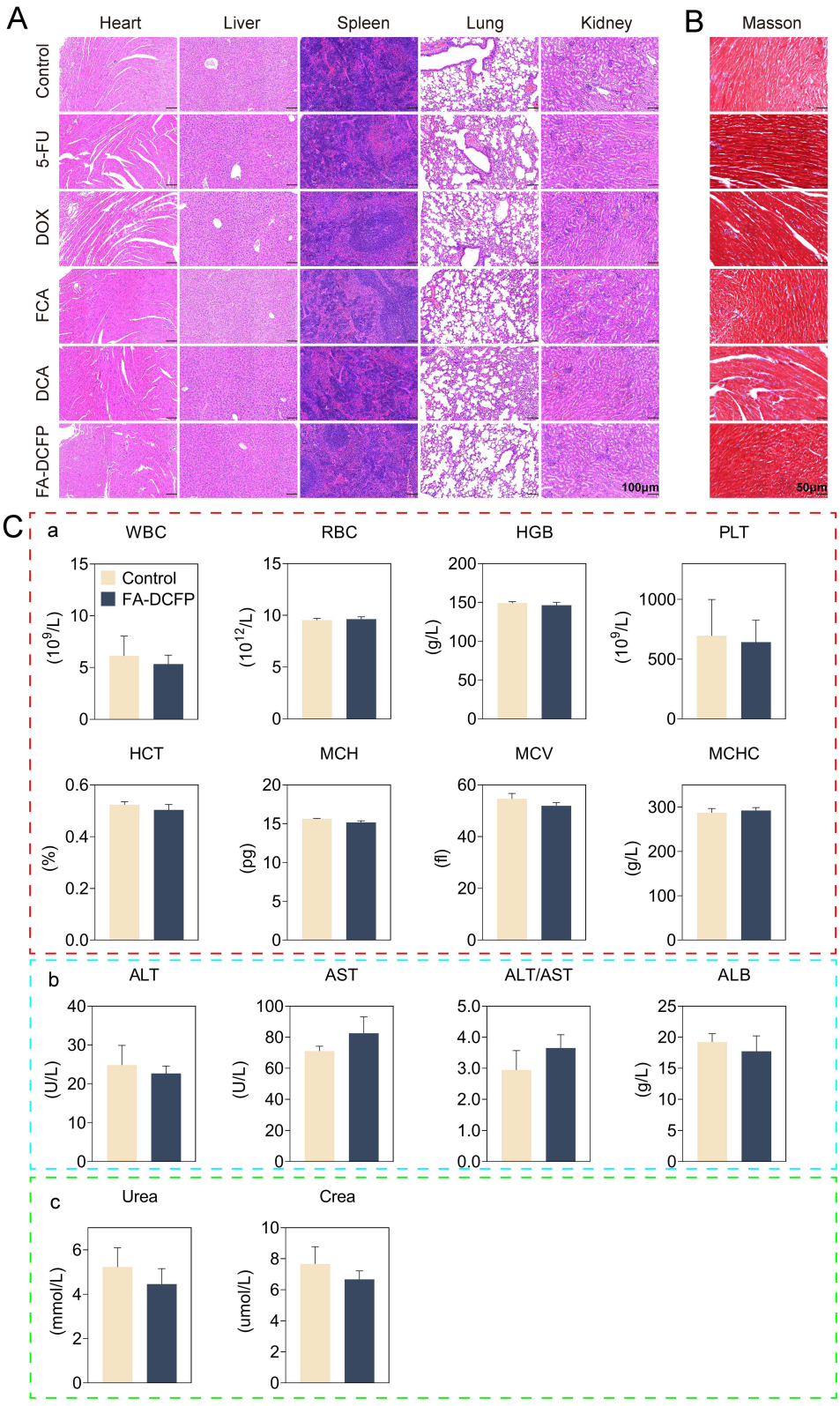

Figure 7 Biocompatibility Assessment. (**A**) Hematoxylin and eosin staining of major organs (including heart, liver, spleen, lung and kidney) after treatment as indicated. Scale bar, 100μm. (**B**) Masson staining of heart after treatment as indicated. Scale bar, 50μm. (**C**) The systemic toxicity of various treatments was analyzed in vivo by examining biochemical markers and routine blood indicators. (a) Blood cell analysis. (b) Liver Function. (c) Renal Function (n = 3).

supplementation, confirming receptor-mediated endocytosis. Conversely, FA-DCFP exhibited no significant uptake difference versus free drug in FR-low-expressing normal cells. In vivo fluorescence imaging further revealed efficient and sustained tumor-selective accumulation of FA-conjugated formulations. These findings collectively validate the synergistic targeting efficacy conferred by folate modification.

However, some studies indicate that utilizing a single chemotherapy drug results in limited improvements in anti-tumor outcomes. 5-Fu, a first-line chemotherapy agent for colon cancer, is often combined with other drugs for enhanced efficacy. Recently, the application of combination therapies has led to an increasing number of investigations into the anti-tumor effects of multi-therapy nanoplatforms that target folate receptors. Consequently, we aimed to co-load 5-Fu and DOX into hollow calcium carbonate nanospheres, encapsulated with PDA, and linked to folate as anchoring points. This study investigates the anti-tumor effects of a dual-drug system that targets folate receptors in colon cancer.

In our research model, the dual-drug system (FA-DCFP) targets and aggregates at solid tumor sites through systemic circulation. Under the influence of the acidic tumor microenvironment, the $CaCO_3$ shell disintegrates, releasing the chemotherapy drugs 5-Fu and DOX. On one hand, $CaCO_3$ neutralizes the acidic environment, releasing excess Ca^{2+} and DOX, which work synergistically to reshape the tumor microenvironment and augment anti-tumor activity.[45] On the other hand, the calcium overload induces metabolic disturbances in tumor cells, thereby enhancing oxidative stress and increasing the inhibitory effects of 5-Fu and DOX. In treatment experiments with tumor-bearing mice, the FA-DCFP group exhibited not only enhanced targeting of solid tumors compared to the free 5-Fu and DOX groups but also significantly improved inhibition of tumor proliferation. Throughout the therapeutic regimen, the FA-DCFP formulation demonstrated excellent tolerability without eliciting observable systemic toxicity in murine subjects. This aligns with the trends observed in our in vitro cell experiments.

Overall, we have successfully designed a pH-responsive dual-drug-loaded nanosystem that targets folate, combining biological safety with anti-tumor efficacy, and propose a straightforward and feasible new strategy for precision chemotherapy in colon cancer.

Conclusion

We have developed a new nano-drug delivery system that encapsulates DOX and 5-Fu in $CaCO_3$ nanoparticles and coats the nanoparticles with a FA-modified PDA for colorectal cancer. By taking advantage of the high expression of FR on CT26 and HepG2 cells, FA-modified nanoparticles are actively taken up by tumour cells. At the same time, the acidic characteristics of the tumour microenvironment further enhance the specific release efficiency of the drug in the tumour area. The synergistic chemotherapeutic effect of DOX and 5-Fu, combined with the decomposition of $CaCO_3$ in the tumour area to produce a large amount of Ca^{2+}, which causes calcium overload in the tumour, together promote the apoptosis and death of tumour cells. The FA-targeted drug delivery to the tumour greatly reduces the systemic toxic side effects of chemotherapeutic drugs.

Acknowledgments

All authors made a significant contribution to the work reported, whether that is in the conception, study design, execution, acquisition of data, analysis and interpretation, or in all these areas; took part in drafting, revising or critically reviewing the article; gave final approval of the version to be published; have agreed on the journal to which the article has been submitted; and agree to be accountable for all aspects of the work.

Funding

This work was supported by Luzhou Science and Technology and Talent Work Bureau (Nos.2022-SYF-55).

Disclosure

The authors have no relevant financial or non-financial interests to disclose.

References

1. Lee SW, Lee HL, Han NI. Transarterial infusion of epirubicin and cisplatin combined with systemic infusion of 5-fluorouracil versus transarterial chemoembolization using doxorubicin for unresectable hepatocellular carcinoma with portal vein tumor thrombosis: a retrospective analysis. *Ther Adv Med Oncol*. 2017;9(10):615–626. doi:10.1177/1758834017728018
2. Symmans WF, Wei C, Gould R. Long-term prognostic risk after neoadjuvant chemotherapy associated with residual cancer burden and breast cancer subtype. *J Clin Oncol*. 2017;35(10):1049–1060. doi:10.1200/JCO.2015.63.1010
3. Lück H-J, Du Bois A, Loibl S. Capecitabine plus paclitaxel versus epirubicin plus paclitaxel as first-line treatment for metastatic breast cancer: efficacy and safety results of a randomized, Phase III trial by the AGO Breast Cancer Study Group. *Breast Cancer Res Treat*. 2013;139(3):779–787. doi:10.1007/s10549-013-2589-8
4. Hardaway BW. Adriamycin-associated cardiomyopathy: where are we now? Updates in pathophysiology, dose recommendations, prognosis, and outcomes. *Curr Opin Cardiol*. 2019;34(3):289–295. doi:10.1097/HCO.0000000000000617
5. Hurvitz SA, Hegg R, Chung W-P. Trastuzumab deruxtecan versus trastuzumab emtansine in patients with HER2-positive metastatic breast cancer: updated results from DESTINY-Breast03, a randomised, open-label, Phase 3 trial. *Lancet*. 2023;401(10371):105–117. doi:10.1016/S0140-6736(22)02420-5
6. Liang G, Cao W, Tang D. Nanomedomics. *ACS Nano*. 2024;18(17):10979–11024. doi:10.1021/acsnano.3c11154
7. Ma X, Li S-J, Liu Y. Bioengineered nanogels for cancer immunotherapy. *Chem Soc Rev*. 2022;51(12):5136–5174. doi:10.1039/D2CS00247G
8. Kolishetti N, Dhar S, Valencia PM. Engineering of self-assembled nanoparticle platform for precisely controlled combination drug therapy. *Proc Natl Acad Sci USA*. 2010;107(42):17939–17944. doi:10.1073/pnas.1011368107
9. Wei T, Chen C, Liu J. Anticancer drug nanomicelles formed by self-assembling amphiphilic dendrimer to combat cancer drug resistance. *Proc Natl Acad Sci USA*. 2015;112(10):2978–2983. doi:10.1073/pnas.1418494112
10. Dai J, Li J, Zhang Y. GM-CSF augmented the photothermal immunotherapeutic outcome of self-driving gold nanoparticles against a mouse CT-26 colon tumor model. *Biomater Res*. 2023;27(1):105. doi:10.1186/s40824-023-00430-6
11. Bujalance Fernández J, de la Asunción-Nadal V, Jurado Sánchez B, Escarpa A. Self-disassembling macroporous metal-organic framework-based micromotors with magnetically controlled motion for sequential drug release. *Small Method*. 2025;e2500724. doi:10.1002/smtd.202500724
12. Ranjbar E, Namazi H, Pooresmaeil M. Carboxymethyl starch encapsulated 5-Fu and DOX co-loaded layered double hydroxide for evaluation of its *in vitro* performance as a drug delivery agent. *Int J Biol Macromol*. 2022;201:193–202. doi:10.1016/j.ijbiomac.2021.12.181
13. Xu T, Fan L, Wang L, Ren H, Zhang Q, Sun W. Hierarchical mesoporous silicon and albumin composite microparticles delivering DOX and Fu for liver cancer treatment. *Int J Biol Macromol*. 2024;268(Pt 1):131732. doi:10.1016/j.ijbiomac.2024.131732
14. Yang X, Sun Y, Zhang H. CaCO 3 nanoplatform for cancer treatment: drug delivery and combination therapy. *Nanoscale*. 2024;16(14):6876–6899. doi:10.1039/D3NR05986C
15. Yu J, Wang L, Xie X. Multifunctional nanoparticles codelivering doxorubicin and amorphous calcium carbonate preloaded with indocyanine green for enhanced chemo-photothermal cancer therapy. *Int J Nanomedicine*. 2023;18:323–337. doi:10.2147/IJN.S394896
16. Wu J, Yi S, Cao Y. Dual-driven nanomotors enable tumor penetration and hypoxia alleviation for calcium overload-photo-immunotherapy against colorectal cancer. *Biomaterials*. 2023;302:122332. doi:10.1016/j.biomaterials.2023.122332
17. Walkon LL, Strubbe-Rivera JO, Bazil JN. Calcium overload and mitochondrial metabolism. *Biomolecules*. 2022;12:12.
18. Maleki Dizaj S, Sharifi S, Ahmadian E, Eftekhari A, Adibkia K, Lotfipour F. An update on calcium carbonate nanoparticles as cancer drug/gene delivery system. *Expert Opin Drug Deliv*. 2019;16(4):331–345. doi:10.1080/17425247.2019.1587408
19. Lin J, Huang L, Xiang R, et al. Blood compatibility evaluations of CaCO(3)particles. *Biomed Mater*. 2021;16:5.
20. Chang M, Hou Z, Jin D. Colorectal tumor microenvironment-activated bio-decomposable and metabolizable Cu 2 O@CaCO 3 nanocomposites for synergistic oncotherapy. *Adv Mater*. 2020;32(43):e2004647. doi:10.1002/adma.202004647
21. Hu S, Xia K, Huang X. Multifunctional CaCO(3)@Cur@QTX125@HA nanoparticles for effectively inhibiting growth of colorectal cancer cells. *J Nanobiotechnol*. 2023;21(1):353. doi:10.1186/s12951-023-02104-w
22. Zi Y, Yang K, He J, Wu Z, Liu J, Zhang W. Strategies to enhance drug delivery to solid tumors by harnessing the EPR effects and alternative targeting mechanisms. *Adv Drug Deliv Rev*. 2022;188:114449. doi:10.1016/j.addr.2022.114449
23. Izci M, Maksoudian C, Manshian BB, Soenen SJ. The use of alternative strategies for enhanced nanoparticle delivery to solid tumors. *Chem Rev*. 2021;121(3):1746–1803. doi:10.1021/acs.chemrev.0c00779
24. Tiwari A, Saraf S, Jain A, Panda PK, Verma A, Jain SK. Basics to advances in nanotherapy of colorectal cancer. *Drug Deliv Transl Res*. 2020;10 (2):319–338. doi:10.1007/s13346-019-00680-9
25. Zhao R, Diop-Bove N, Visentin M, Goldman ID. Mechanisms of membrane transport of folates into cells and across epithelia. *Ann Rev Nutr*. 2011;31(1):177–201. doi:10.1146/annurev-nutr-072610-145133
26. Scaranti M, Cojocaru E, Banerjee S, Banerji U. Exploiting the folate receptor α in oncology. *Nat Rev Clin Oncol*. 2020;17(6):349–359. doi:10.1038/s41571-020-0339-5
27. Gandidzanwa S, Beukes N, Joseph SV, etal. The development of folate-functionalised palladium nanoparticles for folate receptor targeting in breast cancer cells. *Nanotechnology*. 2023;34:46.
28. Gonzalez T, Muminovic M, Nano O, Vulfovich M. Folate receptor alpha-a novel approach to cancer therapy. *Int J Mol Sci*. 2024;25(2).
29. Mi X, Hu M, Dong M. Folic acid decorated zeolitic imidazolate framework (ZIF-8) loaded with baicalin as a nano-drug delivery system for breast cancer therapy. *Int J Nanomedicine*. 2021;16:8337–8352. doi:10.2147/IJN.S340764
30. Handali S, Moghimipour E, Kouchak M. New folate receptor targeted nano liposomes for delivery of 5-fluorouracil to cancer cells: strong implication for enhanced potency and safety. *Life Sciences*. 2019;227:39–50. doi:10.1016/j.lfs.2019.04.030
31. Yamagata M, Hasuda K, Stamato T, Tannock IF. The contribution of lactic acid to acidification of tumours: studies of variant cells lacking lactate dehydrogenase. *Br J Cancer*. 1998;77(11):1726–1731. doi:10.1038/bjc.1998.289
32. Zhen W, An S, Wang S. Precise subcellular organelle targeting for boosting endogenous-stimuli-mediated tumor therapy. *Adv Mater*. 2021;33(51): e2101572. doi:10.1002/adma.202101572
33. Gilabert-Oriol R, Ryan GM, Leung AW, Firmino NS, Bennewith KL, Bally MB. Liposomal formulations to modulate the tumour microenvironment and antitumour immune response. *Int J Mol Sci*. 2018;19:10.

34. Dong Y, Yang J, Liu H. Site-specific drug-releasing polypeptide nanocarriers based on dual-pH response for enhanced therapeutic efficacy against drug-resistant tumors. *Theranostics*. 2015;5(8):890–904. doi:10.7150/thno.11821
35. Zhang X, Qin B, Wang M. Dual pH-responsive and tumor-targeted nanoparticle-mediated anti-angiogenesis siRNA delivery for tumor treatment. *Int J Nanomedicine*. 2022;17:953–967. doi:10.2147/IJN.S340926
36. Dai T, Li N, Han F, Zhang H, Zhang Y, Liu Q. AMP-guided tumour-specific nanoparticle delivery via adenosine A1 receptor. *Biomaterials*. 2016;83:37–50. doi:10.1016/j.biomaterials.2016.01.011
37. Whilding L, Vallath S, Maher J. The integrin αvβ6: a novel target for CAR T-cell immunotherapy? *Biochem Soc Transact*. 2016;44(2):349–355. doi:10.1042/BST20150249
38. Xu G, Song Y, Jin H, et al. Molecular engineering of a tumor-targeting thione-derived diketopyrrolopyrrole photosensitizer to attain NIR excitation over 850 nm for efficient dual phototherapy. *Adv Sci*. 2024;e2407727.
39. Kang X, Bu F, Feng W. Dual-cascade responsive nanoparticles enhance pancreatic cancer therapy by eliminating tumor-resident intracellular bacteria. *Adv Mater*. 2022;34(49):e2206765. doi:10.1002/adma.202206765
40. Liu Y, Hu B, Pei X. A Non-G-quadruplex DNA aptamer targeting NCL for diagnosis and therapy in bladder cancer. *Adv Healthc Mater*. 2023;12(20):e2300791. doi:10.1002/adhm.202300791
41. Yoo HS, Park TG. Folate-receptor-targeted delivery of doxorubicin nano-aggregates stabilized by doxorubicin-PEG-folate conjugate. *J Control Release*. 2004;100(2):247–256. doi:10.1016/j.jconrel.2004.08.017
42. Yuan P, Dou G, Liu T. On-demand manipulation of tumorigenic microenvironments by nano-modulator for synergistic tumor therapy. *Biomaterials*. 2021;275:120956. doi:10.1016/j.biomaterials.2021.120956
43. Wei M, Bai J, Shen X. Glutathione-exhausting nanoprobes for NIR-II fluorescence imaging-guided surgery and boosting radiation therapy efficacy via ferroptosis in breast cancer. *ACS Nano*. 2023;17(12):11345–11361. doi:10.1021/acsnano.3c00350
44. Khan S, Madni A, Shah H. Folate decorated lipid chitosan hybrid nanoparticles of 5-fluorouracil for enhanced anticancer efficacy against colon cancer. *Int J Biol Macromol*. 2022;222(Pt A):497–508. doi:10.1016/j.ijbiomac.2022.09.196
45. Zhu Y, Yang Z, Dong Z. CaCO(3)-assisted preparation of pH-Responsive Immune-Modulating Nanoparticles For Augmented Chemo-Immunotherapy. *Nanomicro Lett*. 2020;13(1):29. doi:10.1007/s40820-020-00549-4

International Journal of Nanomedicine

Dovepress
Taylor & Francis Group

Publish your work in this journal

The International Journal of Nanomedicine is an international, peer-reviewed journal focusing on the application of nanotechnology in diagnostics, therapeutics, and drug delivery systems throughout the biomedical field. This journal is indexed on PubMed Central, MedLine, CAS, SciSearch®, Current Contents®/Clinical Medicine, Journal Citation Reports/Science Edition, EMBase, Scopus and the Elsevier Bibliographic databases. The manuscript management system is completely online and includes a very quick and fair peer-review system, which is all easy to use. Visit http://www.dovepress.com/testimonials.php to read real quotes from published authors.

Submit your manuscript here: https://www.dovepress.com/international-journal-of-nanomedicine-journal